

Jansky Very Large Array detections of CO(1–0) emission in HI-absorption-selected galaxies at $z \gtrsim 2$

B. KAUR,¹ N. KANEKAR,¹ M. RAFELSKI,^{2,3} M. NEELEMAN,⁴ J. X. PROCHASKA,^{5,6} AND M. REVALSKI²

¹*National Centre for Radio Astrophysics, Tata Institute of Fundamental Research, Pune University, Pune 411007, India*

²*Space Telescope Science Institute, 3700 San Martin Drive, Baltimore, MD 21218, USA*

³*Department of Physics & Astronomy, Johns Hopkins University, Baltimore, MD 21218, USA*

⁴*Max-Planck-Institut für Astronomie, Königstuhl 17, D-69117, Heidelberg, Germany*

⁵*Department of Astronomy & Astrophysics, UCO/Lick Observatory, University of California, 1156 High Street, Santa Cruz, CA 95064, USA*

⁶*Kavli Institute for the Physics and Mathematics of the Universe (Kavli IPMU), 5-1-5 Kashiwanoha, Kashiwa, 277-8583, Japan*

ABSTRACT

We report a Karl G. Jansky Very Large Array search for redshifted CO(1–0) emission from three HI-absorption-selected galaxies at $z \approx 2$, identified earlier in their CO(3–2) or CO(4–3) emission. We detect CO(1–0) emission from DLA B1228-113 at $z \approx 2.1933$ and DLA J0918+1636 at $z \approx 2.5848$; these are the first detections of CO(1–0) emission in high- z HI-selected galaxies. We obtain high molecular gas masses, $M_{\text{mol}} \approx 10^{11} \times (\alpha_{\text{CO}}/4.36) M_{\odot}$, for the two objects with CO(1–0) detections, which are a factor of $\approx 1.5 - 2$ lower than earlier estimates. We determine the excitation of the mid- J CO rotational levels relative to the $J = 1$ level, r_{J1} , in HI-selected galaxies for the first time, obtaining $r_{31} = 1.00 \pm 0.20$ and $r_{41} = 1.03 \pm 0.23$ for DLA J0918+1636, and $r_{31} = 0.86 \pm 0.21$ for DLA B1228-113. These values are consistent with thermal excitation of the $J = 3, 4$ levels. The excitation of the $J = 3$ level in the HI-selected galaxies is similar to that seen in massive main-sequence and sub-mm galaxies at $z \gtrsim 2$, but higher than that in main-sequence galaxies at $z \approx 1.5$; the higher excitation of the galaxies at $z \gtrsim 2$ is likely to be due to their higher star-formation rate (SFR) surface density. We use Hubble Space Telescope Wide Field Camera 3 imaging to detect the rest-frame near-ultraviolet emission of DLA B1228-113, obtaining an NUV SFR of $4.44 \pm 0.47 M_{\odot} \text{ yr}^{-1}$, significantly lower than that obtained from the total infrared luminosity, indicating significant dust extinction in the $z \approx 2.1933$ galaxy.

Keywords: galaxies: high-redshift—ISM: molecules—galaxies: evolution—quasars: absorption lines

1. INTRODUCTION

The highest HI column density absorption systems in QSO spectra, the damped Lyman- α absorbers (DLAs), arise from gas associated with high-redshift galaxies (e.g. Wolfe et al. 2005). Such absorbers provide a route to identifying high- z galaxies without the luminosity bias that afflicts galaxy samples selected directly via their emission. Understanding the nature of these HI-absorption-selected galaxies is critical for an unbiased understanding of galaxy evolution. Unfortunately, the proximity of the faint foreground galaxy to the bright background QSO has meant that, despite many studies, it has been difficult to even identify, let alone characterize, the high- z , HI-selected galaxies via optical imaging and spectroscopy (e.g. Fumagalli et al. 2015; Krogager et al. 2017).

Recently, the Atacama Large Millimeter/submillimeter Array (ALMA) and the NOthern Extended Millimeter Array (NOEMA) has opened new windows on HI-selected galaxies via their redshifted [CII] $158\mu\text{m}$ and CO emission. Besides the characterization of HI-selected galaxies at intermediate redshifts, $z \approx 0.6$ (e.g. Møller et al. 2018; Kanekar et al. 2018; Péroux et al. 2019; Klitsch et al. 2019), this has resulted in the identification of more than a dozen such galaxies at $z \approx 2$ (Neeleman et al. 2018; Fynbo et al. 2018; Kanekar et al. 2020; Kaur et al. 2022) and $z \approx 4$ (Neeleman

Table 1. JVLA Ka-band observations and results. The columns are (1) the galaxy name, (2) the QSO redshift, (3) the absorption redshift, z_{abs} , (4) the galaxy redshift, z_{gal} , from the higher- J CO lines, (5) the redshifted CO(1–0) line frequency, in GHz, (6) the synthesized beam, in $''\times''$, (7) the RMS noise, in $\mu\text{Jy}/\text{Beam}$, at a velocity resolution of 100 km s^{-1} , (8) the integrated CO line flux density, in Jy km s^{-1} , (9) the CO(1–0) line luminosity, $L'_{\text{CO}(1-0)}$, and (10) the molecular gas mass, M_{mol} , assuming $\alpha_{\text{CO}} = 4.36 \text{ M}_{\odot} (\text{K km s}^{-1} \text{ pc}^2)^{-1}$. For the CO(1–0) non-detection in B0551-366, the last three columns list the 3σ upper limits on $\int S_{\text{CO}} dV$, $L'_{\text{CO}(1-0)}$, and M_{mol} , for an assumed line FWHM of 300 km s^{-1} (Kanekar et al. 2020).

DLA	z_{QSO}	z_{abs}	z_{gal}	ν_{obs} GHz	Beam $''\times''$	RMS _{CO} $\mu\text{Jy}/\text{Beam}$	$\int S_{\text{CO}} dV$ Jy km s^{-1}	$L'_{\text{CO}(1-0)}$ $10^{10} \text{ K km s}^{-1} \text{ pc}^2$	M_{mol} $10^{10} \text{ M}_{\odot}$
B0551-366	2.317	1.9622	1.9615	38.92	5.8×1.6	99	< 0.057	< 1.14	< 5.0
B1228-113	3.528	2.1929	2.1933	36.10	3.1×2.0	94	0.094 ± 0.023	2.29 ± 0.56	10.0 ± 2.4
J0918+1636	3.096	2.5832	2.5848	32.15	2.8×2.3	57	0.082 ± 0.016	2.65 ± 0.51	11.5 ± 2.2

et al. 2017, 2019). Perhaps the most remarkable results from these studies are the large impact parameters to the QSO sightline of the galaxies at $z \approx 4$ (Neeleman et al. 2017, 2019), the high molecular gas masses of the galaxies at $z \approx 2$ (Kanekar et al. 2020), and the identification of a cold, dusty, rotating disk at $z \approx 4.26$ (Neeleman et al. 2020). Multi-wavelength observations are now under way to obtain a detailed understanding of these galaxies, by characterizing their stellar and gas properties, star-formation activity, etc (e.g. Prochaska et al. 2019; Kaur et al. 2021; Klitsch et al. 2022).

For the $z \approx 2$ HI-selected galaxies, the high inferred molecular gas masses, $M_{\text{mol}} \approx (1.3 - 20.7) \times 10^{10} \text{ M}_{\odot}$ (Kanekar et al. 2020), were obtained from the CO(3–2) or CO(4–3) mid- J rotational transitions. These estimates are based on two critical assumptions, sub-thermal excitation of the CO $J = 3$ or $J = 4$ level relative to the $J = 1$ level, and the value of the CO-to-H₂ conversion factor, α_{CO} (e.g. Tacconi et al. 2020). Direct observations of the CO(1–0) line are critical to remove the first of these assumptions, and obtain more accurate molecular gas mass estimates. Combining the CO(1–0) line luminosity with the luminosity in the higher- J CO lines also allows one to determine the CO excitation and thus probe physical conditions in the molecular gas (e.g. Carilli & Walter 2013). Indeed, studies in the local Universe have shown that the CO excitation is related to the value of α_{CO} : high-excitation galaxies like ultra-luminous infrared galaxies (ULIRGs) and QSO hosts have lower α_{CO} values [$\alpha_{\text{CO}} \approx 1.0 \text{ M}_{\odot} (\text{K km s}^{-1} \text{ pc}^2)^{-1}$] than low-excitation objects like the Milky Way and nearby disk galaxies [$\alpha_{\text{CO}} \approx 4.3 \text{ M}_{\odot} (\text{K km s}^{-1} \text{ pc}^2)^{-1}$; e.g. Bolatto et al. 2013].

At high redshifts, CO(1–0) studies have so far only been carried out in bright, emission-selected galaxies, mostly QSO hosts, sub-mm galaxies, lensed galaxies, and massive main-sequence galaxies (e.g. Aravena et al. 2014; Bolatto et al. 2015; Sharon et al. 2016; Riechers et al. 2020). In this *Letter*, we report the first detections of redshifted CO(1–0) emission from HI-selected galaxies at $z \approx 2$, obtained with the Karl G. Jansky Very Large Array (JVLA)¹. We also report Hubble Space Telescope (HST) Wide Field Camera 3 (WFC3) imaging of the rest-frame near-ultraviolet continuum emission for one of the HI-selected galaxies, which shows that the object is a dusty galaxy.

2. OBSERVATIONS, DATA ANALYSIS, AND RESULTS

2.1. JVLA observations and data analysis

We used the JVLA Ka-band receivers in the D-array to search for redshifted CO(1–0) emission from the HI-selected galaxies at $z \approx 1.9615$ towards QSO B0551-366, $z \approx 2.1933$ towards PKS B1228-113, and $z \approx 2.5848$ towards QSO J0918+1636 in 2019 November and December (Proposal ID: VLA/19B-271, PI: N. Kanekar). The three galaxies (hereafter, DLA B0551-366, DLA B1228-113 and DLA J0918+1636) had been earlier detected with ALMA in their CO(4–3) or CO(3–2) emission (Neeleman et al. 2018; Fynbo et al. 2018; Kanekar et al. 2020).

The JVLA observations used the WIDAR correlator in 8-bit mode, with two 1-GHz intermediate frequency (IF) bands, one covering the redshifted CO line frequency for the target galaxy, and two polarizations. Each IF band was divided into eight 128-MHz digital sub-bands, with each sub-band further divided into 512 and 128 channels, for line and off-line sub-bands, respectively. This yielded a velocity coverage of $\approx 800 - 955 \text{ km s}^{-1}$ for the sub-band covering

¹ We assume a flat Λ -cold dark matter cosmology, with $\Omega_{\Lambda} = 0.685$, $\Omega_m = 0.315$, and $H_0 = 67.4 \text{ km s}^{-1} \text{ Mpc}^{-1}$ (Planck Collaboration 2020).

the redshifted CO line frequency, albeit with lower sensitivity at the sub-band edges, and a raw velocity resolution of $\approx 2 \text{ km s}^{-1}$. Observations of the targets were interleaved with runs on nearby phase calibrators every 5 minutes; in addition, a standard flux calibrator was observed once in each session. The on-source times were 2.1 – 5.8 hrs for the three galaxies.

All data were analysed in the Astronomical Image Processing System package (“classic” AIPS; Greisen 2003), using standard procedures. After identifying and editing out malfunctioning antennas and any data affected by systematic errors, we used the calibrator data to determine the antenna-based complex gains and bandpass shapes. The gains and bandpasses were applied to the data for each target, and the calibrated target visibilities then split out into a new data set. For each target, the central channels of each sub-band of this data set were averaged together, and the resulting data sets were imaged to search for any continuum emission in each field. Although continuum emission was detected from two QSOs, only PKS B1228-113 was found to have a sufficient flux density for self-calibration. The self-calibration for PKS B1228-113 followed a standard iterative procedure, with multiple rounds of imaging and phase-only self-calibration, followed by amplitude-and-phase self-calibration and data editing, until neither the image nor the residual visibilities showed any improvement on further self-calibration. The improved complex gains for DLA B1228-113 were applied to the multi-channel data to produce the final calibrated data set for this field.

Next, for each target, the task UVSUB was used to subtract out all continuum emission from the calibrated visibilities. The residual multi-channel visibility data sets were then imaged in the Common Astronomy Software Applications package (CASA version 5.6; McMullin et al. 2007), using natural weighting in the barycentric frame, to produce spectral cubes at velocity resolutions of $50 - 100 \text{ km s}^{-1}$. The full-width-at-half-maximum (FWHM) of the JVLA synthesized beams is $\approx 1.6'' - 5.8''$ for the three targets, larger than the size of the ALMA CO emission (Kanekar et al. 2020); we hence do not expect any of the CO(1–0) emission to be resolved out in the JVLA images. For each galaxy, a CO(1–0) emission spectrum was extracted by taking a cut through its cube at the location of the ALMA CO emission. Finally, in the case of DLA B1228-113 and DLA J0918+1636, which showed detections of CO(1–0) emission at $> 4\sigma$ significance, we also made images of the CO emission, at velocity resolutions matched to the line FWHMs. The observational details and results are summarized in Table 1.

2.2. HST observations and data analysis

The HST WFC3 observations of DLA B1228-113 were carried out in late 2019 (PID: 15882; PI: Kanekar), using the F105W filter to cover the rest-frame NUV stellar continuum from the $z \approx 2.1933$ galaxy. A single orbit was obtained, using a WIDE-7 dither pattern increased by a factor of 3 over the pattern described in the Instrument Science Report (ISR 2016-14; Anderson 2016), in order to obtain cleaner images by dithering over the size of the IR blobs.

The data were calibrated using the new IR filter-dependent sky flats (WFC3 ISR 2021-01; Mack et al. 2021). Image mosaics were made using AstroDrizzle (Hack et al. 2020), drizzling to a scale of $0''.06 \text{ pixel}^{-1}$. TweakReg was used to astrometrically align the image to the GAIA DR2 catalog (Gaia Collaboration et al. 2018), yielding an absolute astrometric uncertainty of $\approx 0''.01$. The effective angular resolution of the HST WFC3 image is $\approx 0.3''$, based on a Gaussian fit to the point spread function (PSF) of the quasar.

2.3. Results

Our JVLA observations yielded detections of CO(1–0) emission at $> 4\sigma$ significance from the HI-selected galaxies at $z \approx 2.1933$ towards PKS B1228-113 and $z \approx 2.5848$ towards QSO J0918+1636. We also obtained an upper limit to the CO(1–0) line luminosity for the $z \approx 1.9615$ galaxy towards QSO B0551-366. Fig. 1 shows the JVLA CO(1–0) spectra of the three HI-selected galaxies, while Fig. 2 shows the CO(1–0) images of DLA B1228-113 and DLA J0918+1636 (in red contours), overlaid on the ALMA CO(3–2) images (white contours), and the HST WFC3 images (in colour; Fynbo et al. 2018, this work) of the two fields. For DLA B1228-113 and DLA J0918+1636, the detected CO(1–0) emission agrees in both position and velocity with the ALMA CO(3–2) emission. The measured velocity-integrated CO(1–0) line flux densities and inferred CO line luminosities for the three galaxies are listed in Table 1. Here, the 3σ upper limits for DLA B0551-366 assume that the CO(1–0) emission has an FWHM of 300 km s^{-1} , equal to that of the CO(4–3) emission (Kanekar et al. 2020). The CO(1–0) line luminosities yield molecular gas masses of $(10.0 \pm 2.4) \times (\alpha_{\text{CO}}/4.36) \times 10^{10} \text{ M}_{\odot}$ (DLA B1228-113), $(11.5 \pm 2.2) \times (\alpha_{\text{CO}}/4.36) \times 10^{10} \text{ M}_{\odot}$ (DLA J0918+1636) and $< 5.0 \times (\alpha_{\text{CO}}/4.36) \times 10^{10} \text{ M}_{\odot}$ (3σ limit; DLA B0551-366), where we have assumed $\alpha_{\text{CO}} = 4.36 \text{ M}_{\odot} (\text{K km s}^{-1} \text{ pc}^2)^{-1}$ (Bolatto et al. 2013; Tacconi et al. 2020).

Both DLA J0918+1636 and DLA B1228-113 are detected in HST rest-frame NUV imaging. The HST images of DLA J0918+1636 are presented and described in Fynbo et al. (2018), and yield a half-light radius of $0''.30$ (Fynbo,

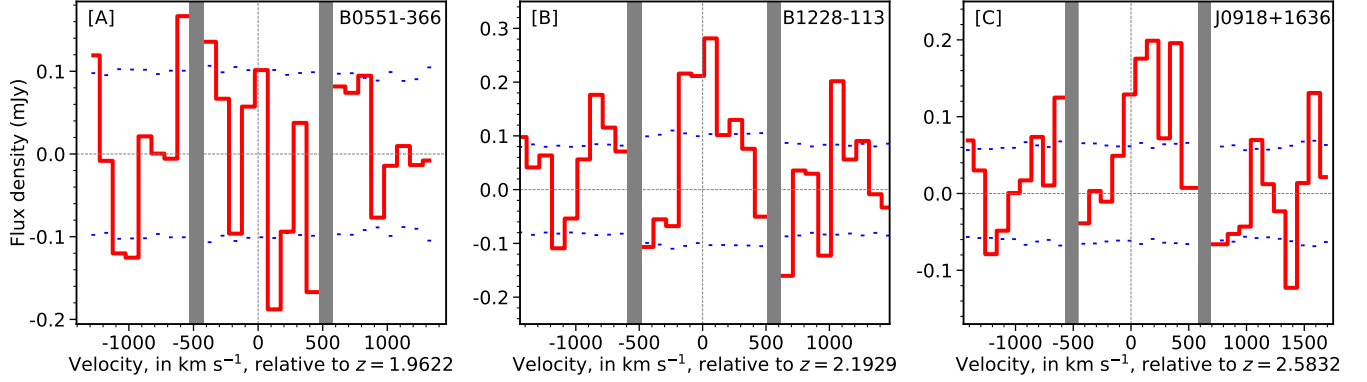


Figure 1. JVLA CO(1–0) spectra from [A] DLA B0551-366 at $z = 1.9615$, [B] DLA B1228-113 at $z = 2.1933$, and [C] DLA J0918+1636 at $z = 2.5848$. The vertical grey bands indicate the edges of the digital sub-bands of the WIDAR correlator, which have significantly lower sensitivity. The blue dashed curves in each panel indicate the $\pm 1\sigma$ error at each velocity channel.

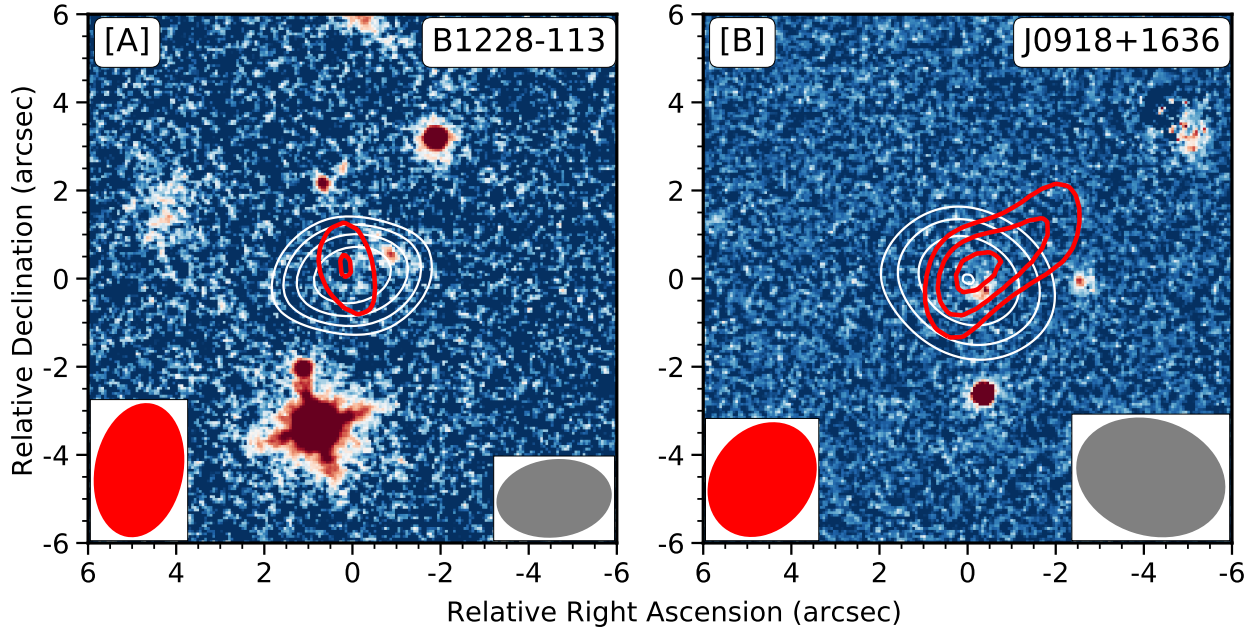


Figure 2. JVLA CO(1–0) integrated emission (red contours) overlaid on the ALMA CO(3–2) emission (white contours) and the HST WFC3 F105W image (in colour) for [A] DLA B1228-113 at $z = 2.1933$ and [B] J0918+1636 at $z = 2.5848$ respectively. The left and right insets in each panel show, respectively, the JVLA (red) and ALMA (grey) synthesized beams. The CO(1–0) contours are at $(-3.0, 3.0, 4.0, 5.0) \times \sigma$ significance (note that there are no negative contours with $\geq 3\sigma$ significance), while the outermost CO(3–2) contour is at 6σ significance, with successive later contours increasing by factors of $\sqrt{2}$.

private communication). In the case of DLA B1228-113, the rest-frame NUV emission is detected in our HST WFC3 F105W image (see Fig. 2[A]), at RA=12h30m55.44s, Dec.=−11°39′05.87″, at an offset of $\approx 0''.9$ (≈ 7.7 kpc) from the CO(3–2) emission. We emphasize that no rest-frame NUV emission is detected at the center of the CO emission (see the discussion in Section 3).

We obtained photometry of DLA B1228-113 using Source Extractor v.2.19.5 (Bertin & Arnouts 1996), measuring the total flux using $\text{flux}_{\text{auto}}$, which gives the flux within an elliptical aperture with the Kron radius (Kron 1980). This yielded an AB magnitude of $m_{\text{AB}} \approx 24.72 \pm 0.12$, a half-light radius of $0''.33$, and a Kron radius of $0''.46$. To infer the SFR of the galaxy, we assume that it has a Chabrier initial mass function (Chabrier 2003) and a flat spectrum in L_ν between rest-frame wavelengths of $\approx 3280\text{\AA}$ and 2300\AA (Kennicutt 1998). Applying the local relation between rest-frame NUV 2300\AA luminosity and SFR (Kennicutt & Evans 2012) then yields an SFR of $4.44 \pm 0.47 M_\odot \text{ yr}^{-1}$.

Table 2. The CO excitation of the three HI-selected galaxies at $z \approx 2$. The columns are (1) the galaxy name, (2) the galaxy redshift, z_{gal} , (3) the ratio r_{31} , (4) the ratio r_{41} , (5) the ratio r_{51} , (6) the ratio r_{61} , and (7) references for the higher- J CO studies.

DLA	z_{gal}	r_{31}	r_{41}	r_{51}	r_{61}	Refs.
B0551-366	1.9615	—	> 0.48	> 0.24	> 0.07	1,2
B1228-113	2.1933	0.86 ± 0.21	—	—	0.18 ± 0.05	1–3
J0918+1636	2.5848	1.00 ± 0.20	1.03 ± 0.23	0.39 ± 0.09	—	1,2,4

(1) Kanekar et al. (2020), (2) Klitsch et al. (2022), (3) Neeleman et al. (2018), (4) Fynbo et al. (2018).

Finally, we combined the rest-frame NUV half-light radii of DLA B1228-113 ($r_{1/2} = 0''.33$) and DLA J0918+1636 ($r_{1/2} = 0''.30$) with the galaxy SFRs ($87 \text{ M}_{\odot} \text{ yr}^{-1}$ and $229 \text{ M}_{\odot} \text{ yr}^{-1}$, obtained from SED fits; Klitsch et al. 2022), to obtain SFR surface densities of $1.8 \text{ M}_{\odot} \text{ yr}^{-1} \text{ kpc}^2$ (DLA B1228-113) and $6.2 \text{ M}_{\odot} \text{ yr}^{-1} \text{ kpc}^2$ (DLA J0918+1636).

3. DISCUSSION

3.1. Molecular gas masses

We have obtained the first detections of CO(1–0) emission in high-redshift HI-selected galaxies. The measured CO(1–0) line luminosities yield direct estimates of the molecular gas mass, without the need for assumptions regarding the CO excitation. We continue to obtain high molecular gas masses in DLA B1228-113 and DLA J0918+1636, albeit a factor of ≈ 1.5 lower than the estimates from the CO(3–2) line (Neeleman et al. 2018; Fynbo et al. 2018; Kanekar et al. 2020). For DLA B0551-366, we have placed an upper limit on its CO(1–0) line luminosity, and thus, on its molecular gas mass, $M_{\text{mol}} < 5.0 \times (\alpha_{\text{CO}}/4.36) \times 10^{10} \text{ M}_{\odot}$. This upper limit is again slightly lower than (but, given the uncertainties, consistent with) the estimate $M_{\text{mol}} = (5.67 \pm 0.68) \times (\alpha_{\text{CO}}/4.36) \times 10^{10} \text{ M}_{\odot}$, obtained by Kanekar et al. (2020) from the CO(4–3) line.

Our molecular gas masses, inferred from the CO(1–0) line, are thus systematically lower, by a factor of ≈ 1.5 , than the values obtained from the mid- J rotational lines (Kanekar et al. 2020). This indicates that the three HI-selected galaxies do not have substantial amounts of cold, low-excitation molecular gas (e.g. Papadopoulos et al. 2001). The lower gas mass estimates obtained here are because the earlier studies assumed sub-thermal excitation of the mid- J CO rotational levels to estimate the CO(1–0) line luminosity, and thence the molecular gas mass.

The main remaining uncertainty in the molecular gas mass estimates for our HI-selected galaxies is the value of the CO-to- H_2 conversion factor, α_{CO} . Estimates of the stellar mass and SFR from fits to the broad-band spectral energy distribution (SED; Klitsch et al. 2022) find that both DLA B1228-113 and DLA J0918+1636 lie slightly ($\approx 0.5 - 0.6$ dex) above the galaxy main sequence at their redshifts, but within the spread of the main sequence (e.g. Whitaker et al. 2012; Schreiber et al. 2015), especially given the large errors in the current SFR estimates. Thus, at present, there is no significant evidence that DLA B1228-113 or DLA J0918+1636 are starburst galaxies, that might have $\alpha_{\text{CO}} \ll 4 \text{ M}_{\odot} (\text{K km s}^{-1} \text{ pc}^2)^{-1}$ (e.g. Magdis et al. 2012). Further, the galaxy metallicities inferred from the stellar mass – metallicity relation at $z \approx 2$ are consistent with solar metallicity (Klitsch et al. 2022). We will hence assume $\alpha_{\text{CO}} \approx 4.36 \text{ M}_{\odot} (\text{K km s}^{-1} \text{ pc}^2)^{-1}$ for these systems (e.g. Bolatto et al. 2013; Tacconi et al. 2020), applicable to high- z main-sequence galaxies with solar metallicity.

Combining the SFR estimates of Klitsch et al. (2022) with our molecular gas mass estimates, we obtain a molecular gas depletion timescale $\tau_{\text{dep}, \text{H}_2} \approx 1.1 \text{ Gyr}$ (DLA B1228-113) and $\approx 0.5 \text{ Gyr}$ (DLA J0918+1636). These are factors of $\approx 2 - 4$ higher than the expected depletion times ($\approx 0.25 \text{ Gyr}$) from the scaling relation of Tacconi et al. (2020).

3.2. The CO spectral line energy distribution (SLED) in HI-selected galaxies

Our JVLA CO(1–0) measurements allow us, for the first time, to determine the excitation of the mid- J rotational levels relative to the $J = 1$ level in HI-selected galaxies. Table 2 lists the values of $r_J \equiv L'_{\text{CO}[J \rightarrow (J-1)]}/L'_{\text{CO}(1-0)}$, for $J = 3 - 6$, combining our measured CO(1–0) line luminosities with the luminosities of the higher- J lines (Kanekar et al. 2020; Klitsch et al. 2022).

Studies of high-redshift galaxies typically assume sub-thermal excitation of the mid- J rotational levels, with $r_{31} \approx 0.55$ and $r_{41} \approx 0.42$ (e.g. Tacconi et al. 2020). Remarkably, we find that DLA J0918+1636 has values of $r_{31} = 1.00 \pm 0.20$ and $r_{41} = 1.03 \pm 0.23$, consistent with thermal excitation of the $J = 3, 4$ levels. We note that Klitsch et al. (2022) had earlier measured $r_{43} = 1.03$ in DLA J0918+1636, suggesting that the $J = 4$ and $J = 3$ levels are likely to show thermal

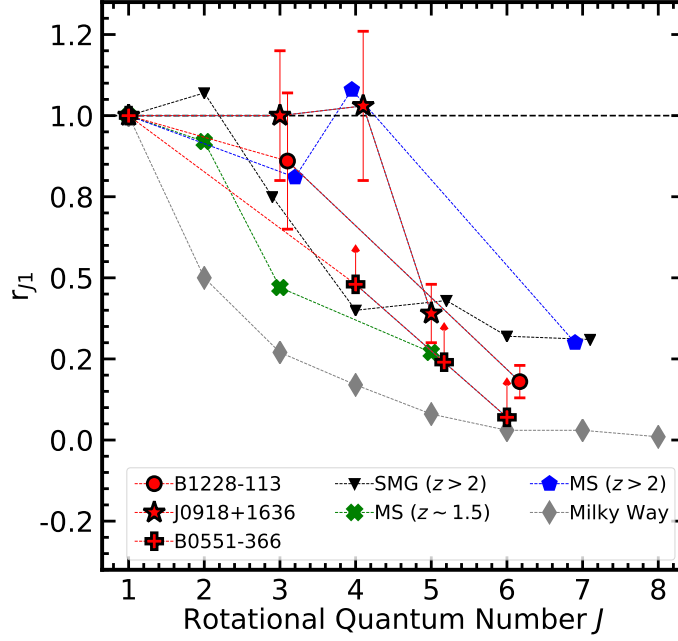


Figure 3. The ratio of the CO($J \rightarrow J - 1$) line luminosity to the CO(1-0) line luminosity, plotted as a function of the upper-state rotational quantum number, J . The dashed black line indicates the value of unity for thermal excitation. The red symbols represent the HI-selected galaxies at $z \sim 2$ (Kanekar et al. 2020; Klitsch et al. 2022, this work). For comparison, we have plotted the median value of the above ratios for main-sequence galaxies at $z \approx 1.5$ (green crosses; Daddi et al. 2015), main-sequence galaxies at $z > 2$ (blue pentagons; Riechers et al. 2010; Brisbin et al. 2019; Boogaard et al. 2020; Henríquez-Brocal et al. 2021), and submillimetre galaxies at $z > 2$ (inverted black triangles; Sharon et al. 2016; Calistro Rivera et al. 2018; Birkin et al. 2021). The grey diamonds indicate the CO SLED of the inner disk of the Milky Way (Fixsen et al. 1999).

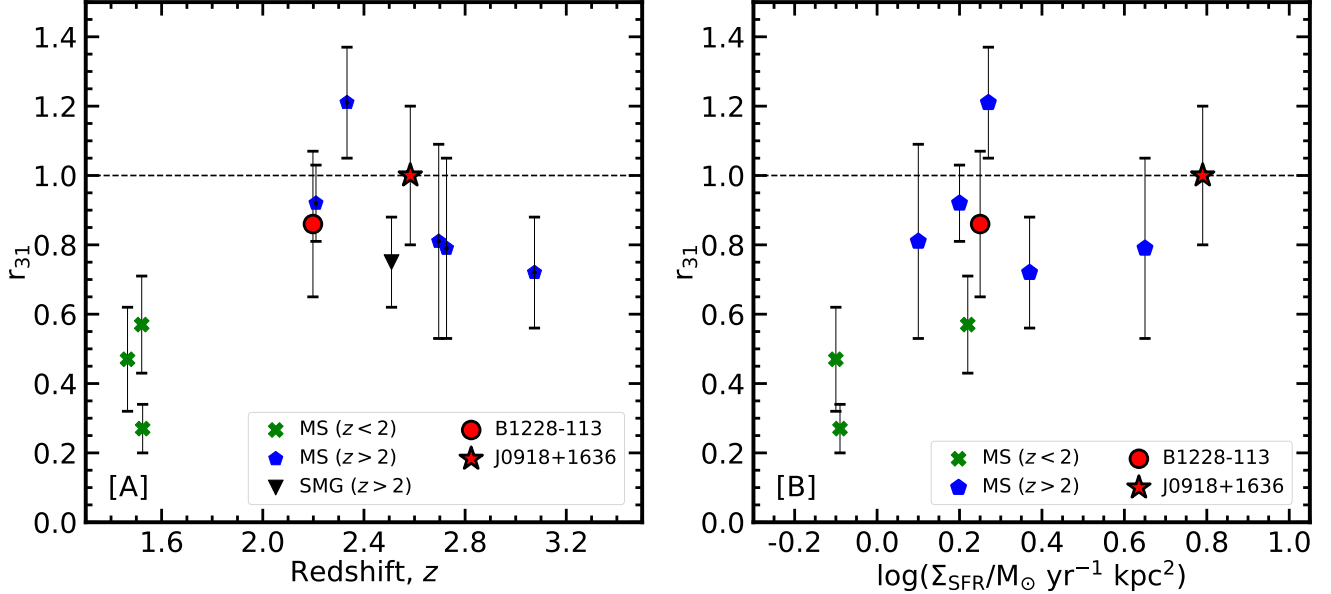


Figure 4. The ratio of the CO(3-2) line luminosity to the CO(1-0) line luminosity (r_{31}), plotted as a function of [A] redshift and [B] SFR surface density, for the HI-selected galaxies of this work (red symbols), BzK galaxies at $z \approx 1.5$ (green crosses; Daddi et al. 2015), and main-sequence galaxies at $z > 2$ (blue pentagons; Riechers et al. 2010; Brisbin et al. 2019; Boogaard et al. 2020; Henríquez-Brocal et al. 2021). The left panel also shows the median r_{31} value for submillimetre galaxies at $z > 2$ (inverted black triangles; Sharon et al. 2016). The dashed horizontal line in both panels indicate $r_{31} = 1$, for thermal excitation.

excitation. Similarly, the value of $r_{31} = 0.86 \pm 0.21$ in DLA B1228-113 is consistent with thermal excitation, while the CO(1–0) non-detection in DLA B0551-366 yields the lower limit $r_{41} > 0.48$, higher than the canonical value of 0.42 (Tacconi et al. 2020). We thus find direct evidence that the mid- J rotational levels of massive HI-selected galaxies at $z \gtrsim 2$ show relatively high excitation (see also Klitsch et al. 2022).

Fig. 3 plots the r_{J1} values of the three HI-selected galaxies (red symbols) against the upper rotational level quantum number, J . The dashed horizontal line at $r_{J1} = 1$ indicates thermal excitation of the rotational levels. The figure also includes data for the inner disk of the Milky Way (grey diamonds; Fixsen et al. 1999), three main-sequence (BzK) galaxies at $z \approx 1.5$ (green crosses; Aravena et al. 2014; Daddi et al. 2015), five main-sequence galaxies at $z > 2$ (blue pentagons; Riechers et al. 2010; Bolatto et al. 2015; Brisbin et al. 2019; Boogaard et al. 2020; Riechers et al. 2020; Henríquez-Brocal et al. 2021), and a large sample of sub-mm galaxies (SMGs) at $z > 2$ (inverted black triangles; Birkin et al. 2021). For the high- z main-sequence galaxies and SMGs, the figure shows the median values of r_{J1} of objects with measurements of both the CO(1–0) line and higher- J CO lines. In the case of the SMGs, we have used the median CO SLED of the large SMG sample of Birkin et al. (2021), who assumed $r_{21} = 0.9$ due to the paucity of CO(1–0) measurements in their sample. We bypass this assumption by normalizing their r_{J1} values to $r_{31} = 0.75$, the median measured r_{31} value obtained for 18 SMGs at $z \approx 2.2 - 3.1$ (Sharon et al. 2016; Calistro Rivera et al. 2018).

Fig. 3 shows that the three HI-selected galaxies have CO SLEDs consistent with those of massive main-sequence galaxies at $z > 2$. The excitation of the mid- J rotational levels of the HI-selected galaxies is clearly higher than that of both the inner disk of the Milky Way and main-sequence galaxies at $z \approx 1.5$. Further, the roughly thermal excitation of the $J = 3, 4$ levels in DLA J0918+1636 (and of the $J = 3$ level in DLA B1228-113) is consistent with the excitation of the same levels in the main-sequence galaxy BX610 (Bolatto et al. 2015; Brisbin et al. 2019). It is interesting that the excitation in DLA J0918+1636 drops sharply in the $J = 5$ rotational level, with $r_{51} \approx 0.39$, well below thermal.

Fig. 4[A] plots r_{31} versus redshift for DLA B1228-113, DLA J0918+1636, and the above samples of SMGs at $z > 2$, and main-sequence galaxies at $z \approx 1.5$ and $z > 2$. Here, the individual r_{31} values are plotted for the main-sequence galaxies (e.g. Riechers et al. 2010; Daddi et al. 2015; Bolatto et al. 2015; Brisbin et al. 2019; Henríquez-Brocal et al. 2021; Boogaard et al. 2020) and the median value for the SMGs (Sharon et al. 2016). Interestingly, we find evidence that all galaxies at $z > 2$ show higher excitation of the $J = 3$ level than main-sequence galaxies at $z \approx 1.5$, by a factor of $\approx 1.5 - 2$. This is consistent with the result from the ALMA Spectroscopic Survey in the Hubble Ultra Deep Field (ASPECS), that galaxies at $z \geq 2$ have an intrinsically higher CO excitation than those at $z < 2$ (Boogaard et al. 2020). As noted by the latter authors, the likely cause of the higher CO excitation is the higher SFR surface density Σ_{SFR} in higher- z galaxies (e.g. Shibuya et al. 2015): simulations have found that the CO excitation is closely linked to the SFR surface density, with a higher excitation obtained for higher values of Σ_{SFR} (Narayanan & Krumholz 2014; Bournaud et al. 2015). Fig. 4[B] plots r_{31} versus SFR surface density for our HI-selected galaxies and the main-sequence galaxies² of the left panel. It is clear that the SFR surface densities of the HI-selected galaxies and the $z > 2$ main-sequence galaxies are higher by factors of $\approx 2 - 10$ than those of the main-sequence galaxies at $z \approx 1.5$, consistent with the higher CO excitation of the higher- z sample.

3.3. Stellar properties of DLA B1228-113

Finally, our SFR estimate of $4.44 \pm 0.47 \text{ M}_{\odot} \text{ yr}^{-1}$ for the $z \approx 2.1933$ HI-selected galaxy DLA B1228-113 from its rest-frame NUV continuum is consistent with the estimate of $\approx 3.9 \text{ M}_{\odot} \text{ yr}^{-1}$ from the H α line (Neeleman et al. 2018). The total SFR, estimated from both the total infrared luminosity and fits to the broadband SED, is far higher than the above estimates, $\approx (87 - 100) \text{ M}_{\odot} \text{ yr}^{-1}$ (Neeleman et al. 2018; Klitsch et al. 2022), implying a high dust extinction. Fig. 2[A] shows that the rest-frame NUV emission detected in the HST WFC3 image is offset from the peak of the ALMA CO(3–2) emission, by $\approx 8 \text{ kpc}$. Combined with the very large CO(3–2) line FWHM ($\approx 600 \text{ km s}^{-1}$; Neeleman et al. 2018), this suggests that the CO emission may arise from two merging galaxies, one of which has a high extinction and is hence not visible in the HST WFC3 image. High angular resolution CO mapping studies would be of much interest to directly probe this issue. Finally, we cannot formally rule out the possibility that the detected NUV emission arises from an interloper at a different redshift; if so, this would imply an even higher dust extinction for the $z \approx 2.1933$ HI-selected galaxy.

4. SUMMARY

² The Σ_{SFR} values for the main-sequence galaxies are from Tacconi et al. (2013) and Boogaard et al. (2020).

We report JVLA detections of CO(1–0) emission in two HI-selected galaxies at $z \approx 2.1933$ and $z \approx 2.5848$, and an upper limit to the CO(1–0) line luminosity in a third HI-selected galaxy at $z \approx 1.9615$. These are the first detections of CO(1–0) emission in HI-selected galaxies at high redshifts, $z \gtrsim 2$, allowing us to directly estimate the molecular gas mass of the galaxies without assumptions about their CO excitation. We obtain molecular gas masses $\approx 1.5 - 2$ times lower than earlier estimates based on the mid- J CO lines. We find thermal excitation of the $J = 3, 4$ rotational levels in the $z = 2.5848$ galaxy DLA J0918+1636, and near-thermal excitation of the $J = 3$ level in the $z = 2.1933$ galaxy DLA B1228-113. In both cases, the CO excitation of the mid- J rotational levels is higher than that typically assumed for main-sequence galaxies at $z \approx 2$. We also find evidence for higher excitation of the $J = 3$ level in HI-selected galaxies, main-sequence galaxies, and SMGs at $z \gtrsim 2$, than in main-sequence galaxies at $z \approx 1.5$. This appears to arise due to a higher SFR surface density in the former types of galaxies. Finally, we used HST WFC3 imaging to detect rest-frame NUV emission from the $z \approx 2.1933$ galaxy DLA B1228-113, obtaining an NUV SFR of $4.44 \pm 0.47 \text{ M}_{\odot} \text{ yr}^{-1}$. This is a factor of ≈ 20 lower than the SFR estimated from the total infrared luminosity or from SED fitting, confirming that the object is a highly dusty galaxy. The stellar NUV emission appears slightly offset from the ALMA CO(3–2) emission, suggesting that the CO and NUV emission may arise from a pair of merging galaxies, one of which is highly obscured and hence not detected in its stellar emission.

Software: DrizzlePac (Hack et al. 2020), CASA (v5.6; McMullin et al. 2007), AIPS (Greisen 2003), ASTROPY (Astropy Collaboration et al. 2013).

We thank Johan Fynbo for providing us with the HST fit results for DLA J0918+1636. BK and NK acknowledge the Department of Atomic Energy for funding support, under project 12-R&D-TFR-5.02-0700. MN acknowledges support from ERC advanced grant 740246 (Cosmic.Gas). This research is based on observations made with the NASA/ESA Hubble Space Telescope obtained from the Space Telescope Science Institute, which is operated by the Association of Universities for Research in Astronomy, Inc., under NASA contract NAS 5–26555. Support for Program number 15882 was provided through a grant from the STScI under NASA contract NAS5-26555. The National Radio Astronomy Observatory is a facility of the National Science Foundation operated under cooperative agreement by Associated Universities, Inc. This material is based upon work supported by the National Science Foundation under Grant No. 2107989.

REFERENCES

- Anderson, J. 2016, Supplemental Dither Patterns for WFC3/IR, Space Telescope WFC Instrument Science Report
- Aravena, M., Hodge, J. A., Wagg, J., et al. 2014, MNRAS, 442, 558, doi: [10.1093/mnras/stu838](https://doi.org/10.1093/mnras/stu838)
- Astropy Collaboration, Robitaille, T. P., Tollerud, E. J., et al. 2013, A&A, 558, A33, doi: [10.1051/0004-6361/201322068](https://doi.org/10.1051/0004-6361/201322068)
- Bertin, E., & Arnouts, S. 1996, A&AS, 117, 393, doi: [10.1051/aas:1996164](https://doi.org/10.1051/aas:1996164)
- Birkin, J. E., Weiss, A., Wardlow, J. L., et al. 2021, MNRAS, 501, 3926, doi: [10.1093/mnras/staa3862](https://doi.org/10.1093/mnras/staa3862)
- Bolatto, A. D., Wolfire, M., & Leroy, A. K. 2013, ARA&A, 51, 207, doi: [10.1146/annurev-astro-082812-140944](https://doi.org/10.1146/annurev-astro-082812-140944)
- Bolatto, A. D., Warren, S. R., Leroy, A. K., et al. 2015, ApJ, 809, 175, doi: [10.1088/0004-637X/809/2/175](https://doi.org/10.1088/0004-637X/809/2/175)
- Boogaard, L. A., van der Werf, P., Weiss, A., et al. 2020, ApJ, 902, 109, doi: [10.3847/1538-4357/abb82f](https://doi.org/10.3847/1538-4357/abb82f)
- Bournaud, F., Daddi, E., Weiß, A., et al. 2015, A&A, 575, A56, doi: [10.1051/0004-6361/201425078](https://doi.org/10.1051/0004-6361/201425078)
- Brisbin, D., Aravena, M., Daddi, E., et al. 2019, A&A, 628, A104, doi: [10.1051/0004-6361/201935148](https://doi.org/10.1051/0004-6361/201935148)
- Calistro Rivera, G., Hodge, J. A., Smail, I., et al. 2018, ApJ, 863, 56, doi: [10.3847/1538-4357/aacffa](https://doi.org/10.3847/1538-4357/aacffa)
- Carilli, C. L., & Walter, F. 2013, ARA&A, 51, 105, doi: [10.1146/annurev-astro-082812-140953](https://doi.org/10.1146/annurev-astro-082812-140953)
- Chabrier, G. 2003, ApJL, 586, L133, doi: [10.1086/374879](https://doi.org/10.1086/374879)
- Daddi, E., Dannerbauer, H., Liu, D., et al. 2015, A&A, 577, A46, doi: [10.1051/0004-6361/201425043](https://doi.org/10.1051/0004-6361/201425043)
- Fixsen, D. J., Bennett, C. L., & Mather, J. C. 1999, ApJ, 526, 207, doi: [10.1086/307962](https://doi.org/10.1086/307962)
- Fumagalli, M., O’Meara, J. M., Prochaska, J. X., Rafelski, M., & Kanekar, N. 2015, MNRAS, 446, 3178, doi: [10.1093/mnras/stu2325](https://doi.org/10.1093/mnras/stu2325)
- Fynbo, J. P. U., Heintz, K. E., Neeleman, M., et al. 2018, MNRAS, 479, 2126, doi: [10.1093/mnras/sty1520](https://doi.org/10.1093/mnras/sty1520)
- Gaia Collaboration, Brown, A. G. A., Vallenari, A., et al. 2018, A&A, 616, A1, doi: [10.1051/0004-6361/201833051](https://doi.org/10.1051/0004-6361/201833051)

- Greisen, E. W. 2003, in *Astrophysics and Space Science Library*, Vol. 285, *Information Handling in Astronomy - Historical Vistas*, ed. A. Heck (Kluwer, Dordrecht), 109, doi: [10.1007/0-306-48080-8_7](https://doi.org/10.1007/0-306-48080-8_7)
- Hack, W. J., Cara, M., Sosey, M., et al. 2020, doi: [10.5281/zenodo.3743274](https://doi.org/10.5281/zenodo.3743274)
- Henríquez-Brocal, K., Herrera-Camus, R., Tacconi, L., et al. 2021, arXiv e-prints, arXiv:2109.01684. <https://arxiv.org/abs/2109.01684>
- Kanekar, N., Prochaska, J., Neeleman, M., et al. 2020, ApJL, 901, L5. <https://arxiv.org/abs/2009.04001>
- Kanekar, N., Prochaska, J. X., Christensen, L., et al. 2018, ApJL, 856, L23, doi: [10.3847/2041-8213/aab6ab](https://doi.org/10.3847/2041-8213/aab6ab)
- Kaur, B., Kanekar, N., Rafelski, M., et al. 2021, ApJ, 921, 68, doi: [10.3847/1538-4357/ac12d2](https://doi.org/10.3847/1538-4357/ac12d2)
- Kaur, B., Kanekar, N., Revalski, M., et al. 2022, arXiv e-prints, arXiv:2206.10623. <https://arxiv.org/abs/2206.10623>
- Kennicutt, Robert C., J. 1998, ARA&A, 36, 189, doi: [10.1146/annurev.astro.36.1.189](https://doi.org/10.1146/annurev.astro.36.1.189)
- Kennicutt, R. C., & Evans, N. J. 2012, ARA&A, 50, 531, doi: [10.1146/annurev-astro-081811-125610](https://doi.org/10.1146/annurev-astro-081811-125610)
- Klitsch, A., Zwaan, M. A., Péroux, C., et al. 2019, MNRAS, 482, L65, doi: [10.1093/mnras/sly187](https://doi.org/10.1093/mnras/sly187)
- Klitsch, A., Christensen, L., Valentino, F., et al. 2022, MNRAS, 514, 2346, doi: [10.1093/mnras/stac1190](https://doi.org/10.1093/mnras/stac1190)
- Krogager, J. K., Møller, P., Fynbo, J. P. U., & Noterdaeme, P. 2017, MNRAS, 469, 2959, doi: [10.1093/mnras/stx1011](https://doi.org/10.1093/mnras/stx1011)
- Kron, R. G. 1980, ApJS, 43, 305, doi: [10.1086/190669](https://doi.org/10.1086/190669)
- Mack, J., Olszewski, H., & Pirzkal, N. 2021, WFC3/IR Filter-Dependent Sky Flats, Space Telescope WFC Instrument Science Report
- Magdis, G. E., Daddi, E., Béthermin, M., et al. 2012, ApJ, 760, 6, doi: [10.1088/0004-637X/760/1/6](https://doi.org/10.1088/0004-637X/760/1/6)
- McMullin, J. P., Waters, B., Schiebel, D., Young, W., & Golap, K. 2007, in *Astronomical Society of the Pacific Conference Series*, Vol. 376, *Astronomical Data Analysis Software and Systems XVI*, ed. R. A. Shaw, F. Hill, & D. J. Bell, 127
- Møller, P., Christensen, L., Zwaan, M. A., et al. 2018, MNRAS, 474, 4039, doi: [10.1093/mnras/stx2845](https://doi.org/10.1093/mnras/stx2845)
- Narayanan, D., & Krumholz, M. R. 2014, MNRAS, 442, 1411, doi: [10.1093/mnras/stu834](https://doi.org/10.1093/mnras/stu834)
- Neeleman, M., Kanekar, N., Prochaska, J. X., et al. 2018, ApJL, 856, L12, doi: [10.3847/2041-8213/aab5b1](https://doi.org/10.3847/2041-8213/aab5b1)
- . 2017, Science, 355, 1285, doi: [10.1126/science.aal1737](https://doi.org/10.1126/science.aal1737)
- Neeleman, M., Kanekar, N., Prochaska, J. X., Rafelski, M. A., & Carilli, C. L. 2019, ApJL, 870, L19, doi: [10.3847/2041-8213/aaf871](https://doi.org/10.3847/2041-8213/aaf871)
- Neeleman, M., Prochaska, J. X., Nissim, K., & Rafelski, M. 2020, Nature, 581, 269, doi: [10.1038/s41586-020-2276-y](https://doi.org/10.1038/s41586-020-2276-y)
- Papadopoulos, P., Ivison, R., Carilli, C., & Lewis, G. 2001, Nature, 409, 58, doi: [10.1038/35051029](https://doi.org/10.1038/35051029)
- Péroux, C., Zwaan, M. A., Klitsch, A., et al. 2019, MNRAS, 485, 1595, doi: [10.1093/mnras/stz202](https://doi.org/10.1093/mnras/stz202)
- Planck Collaboration. 2020, A&A, 641, A6, doi: [10.1051/0004-6361/201833910](https://doi.org/10.1051/0004-6361/201833910)
- Prochaska, J. X., Neeleman, M., Kanekar, N., & Rafelski, M. 2019, ApJL, 886, L35, doi: [10.3847/2041-8213/ab55eb](https://doi.org/10.3847/2041-8213/ab55eb)
- Riechers, D. A., Carilli, C. L., Walter, F., & Momjian, E. 2010, ApJL, 724, L153, doi: [10.1088/2041-8205/724/2/L153](https://doi.org/10.1088/2041-8205/724/2/L153)
- Riechers, D. A., Boogaard, L. A., Decarli, R., et al. 2020, ApJL, 896, L21, doi: [10.3847/2041-8213/ab9595](https://doi.org/10.3847/2041-8213/ab9595)
- Schreiber, C., Pannella, M., Elbaz, D., et al. 2015, A&A, 575, A74, doi: [10.1051/0004-6361/201425017](https://doi.org/10.1051/0004-6361/201425017)
- Sharon, C. E., Riechers, D. A., Hodge, J., et al. 2016, ApJ, 827, 18, doi: [10.3847/0004-637X/827/1/18](https://doi.org/10.3847/0004-637X/827/1/18)
- Shibuya, T., Ouchi, M., & Harikane, Y. 2015, ApJS, 219, 15, doi: [10.1088/0067-0049/219/2/15](https://doi.org/10.1088/0067-0049/219/2/15)
- Tacconi, L. J., Genzel, R., & Sternberg, A. 2020, ARA&A, 58, 157, doi: [10.1146/annurev-astro-082812-141034](https://doi.org/10.1146/annurev-astro-082812-141034)
- Tacconi, L. J., Neri, R., Genzel, R., et al. 2013, ApJ, 768, 74, doi: [10.1088/0004-637X/768/1/74](https://doi.org/10.1088/0004-637X/768/1/74)
- Whitaker, K. E., van Dokkum, P. G., Brammer, G., & Franx, M. 2012, ApJL, 754, L29, doi: [10.1088/2041-8205/754/2/L29](https://doi.org/10.1088/2041-8205/754/2/L29)
- Wolfe, A. M., Gawiser, E., & Prochaska, J. X. 2005, ARA&A, 43, 861, doi: [10.1146/annurev.astro.42.053102.133950](https://doi.org/10.1146/annurev.astro.42.053102.133950)